Fall 2021

Operating Strategies and Disturbance Characterization for DC Microgrids

Miles Leonard-Albert

Operating Strategies and Disturbance Characterization for DC Microgrids

by

Miles Leonard-Albert

Bachelor of Science in Engineering
University of South Carolina 2019

Bachelor of Arts
University of South Carolina 2019

Submitted in Partial Fulfillment of the Requirements

for the Degree of Master of Science in

Electrical Engineering

College of Engineering and Computing

University of South Carolina

2021

Accepted by:

Kristen Booth, Director of Thesis

Roger Dougal, Reader

Tracey L. Weldon, Interim Vice Provost and Dean of the Graduate School

Acknowledgments

The author appreciates the support of the Office of Naval Research on a project that compliments this thesis' work.

Abstract

The present state of the electrical grid is unable to meet the demands of transmission. Digital twin technology provides a promising solution to this problem by allowing for analysis and control of distributed energy resources. This thesis presents initial work towards development of a digital twin for a DC power system. Two versions of the DC power system are created and evaluated against randomly generated load profiles. System performance is evaluated on the basis of the quantity of the load that is unserviced by the generation and energy storage. Energy storage operating strategies that modify the model to prioritize different aspects of the system are introduced, along with a discussion of the effects of the modifications. A preliminary optimization function is discussed that will be used to control the system. From this optimization function, key information that is needed for the digital twin can be determined. This work also introduces two additional works that will require adjustments as the digital twin is developed. The first measures the ability of the system to withstand disturbances. The second presents a decision matrix to examine the trade-off between the number of pulses that the system is capable of producing and the magnitude of those pulses.

Table of Contents

Acknowledgments iii

Abstract iv

List of Tables vii

List of Figures viii

Chapter 1 Introduction 1

1.1 Research Goal and Main Contribution of Thesis 2

1.2 Thesis Structure 2

Chapter 2 Background Literature 4

2.1 Digital Twin Modeling 4

2.2 DC Power Systems 6

2.3 Energy Storage 7

2.4 Power Flow Optimization 7

Chapter 3 Methodology and Modeling 9

3.1 Methodology 9

3.2 Lumped-Generation Model 12

3.3 Distributed Resource Model 15

3.4 Modeling Conclusions and Future Works 19

Chapter 4 Energy Storage Operating Strategies 21

4.1 Energy Storage Operating Strategies Configuration 22

4.2 Energy Storage Operating Strategies Results 22

4.3 Changing Energy Storage Operating Strategies 23

4.4 ESOS Conclusions and Future Works 28

Chapter 5 Optimization and Key Information 29

5.1 Optimization Definition 29

5.2 Optimization Conclusions and Future Works 32

5.3 Power System Key Information 33

Chapter 6 Works in Consideration 34

6.1 Disturbance Management 34

6.2 Pulse Load Decision Matrix 36

Bibliography 40

List of Tables

Table 3.1 Power System Parameters 10

Table 3.2 Lumped-Generation Model Results 15

Table 3.3 Distributed Resource Model Results 18

Table 4.1 Health-Priority Energy Storage Operating Strategy Results 24

Table 4.2 Energy Storage Operating Strategies Change Results 26

Table 6.1 Pulse Profile Definitions 38

Table 6.2 Pulse Load Decision Matrix 39

List of Figures

Figure 3.1 Ten load profiles, meeting the prescribed requirements, used in various studies for this work. 11

Figure 3.2 Case 1 load profile tested in the lumped generation model. First plot: generation vs load. Second plot: energy storage. Third plot: unserviced load. 13

Figure 3.3 Case 1 load profile tested in the distributed resource model. First plot: generation vs load. Second plot: energy storage. Third plot: unserviced load. 17

Figure 4.1 Case 1 load profile tested in the HP-ESOS. First plot: generation vs load. Second plot: energy storage. Third plot: unserviced load. 23

Figure 4.2 Case 8 changing from the HP-ESOS to the PP-ESOS. First plot: generation vs load. Second plot: energy storage. Third plot: unserviced load. 25

Figure 4.3 Case 8 changing from PP-ESOS to the HP-ESOS. First plot: generation vs load. Second plot: energy storage. Third plot: unserviced load. 25

Figure 4.4 ESOS and ESOS-change result comparison. Results reported in percent of energy that is unserviceable throughout the simulation. 27

Figure 6.1 Load disturbance patterns. 35

Figure 6.2 Comparison of ESOS results and results with disturbances. 37

Chapter 1

Introduction

Electricity generation in the United States has grown from 335 TWh in 1950 to 4009 TWh in 2020 according to the U.S. Energy Information Authority [1]. Due to this unexpected increase in generation caused by more loads, the modern distribution grid is not suited to handle the power flowing in the modern system. For instance, the Electric Reliability Council of Texas claims that congestion of the grid costs the state roughly $1 billion per year [2], and Northern Vermont has a moratorium on new renewable energy projects due to grid overload [3]. The insufficiency of the grid is partially due to the relatively stagnant technology, remaining largely unchanged since World War II [4]. Implementation of new technologies, especially distributed energy resources and smart grid monitoring and control schemes, into the grid will help alleviate the issues with stability and capacity. Increased penetration of distributed energy resources will require increased amounts of energy storage integrated into the grid [5]. This can help relieve grid congestion by distributing the generation throughout the system and aid stability by providing increased storage. Companies such as Helia Technologies are developing modules to connect and control generation and storage connected to the grid. Development of systems such as these that improve monitoring, maintenance, and repair of the grid could help mitigate the estimated $25 billion to $70 billion lost per year due to weather related outages [6]. These smart grid technologies are also estimated to reduce carbon emissions by 12 % [7]. Between the economic, environmental, and human factors of grid performance, new technologies to improve power systems are of great benefit. These benefits extend

past the terrestrial grids, including shipboard [8], spacecraft, and extraterrestrial use [9].

1.1 Research Goal and Main Contribution of Thesis

With the goal of developing this smart grid technology, this work presents the modeling, simulations, and results of a DC power system model to be integrated into a digital twin system. This thesis considers two iterations of the model as well as new applications and tests of the model to evaluate loading variations. Additionally, an early version of an optimization algorithm is established.

The main objectives of this work include:

1. Implementing energy storage operating strategies, ESOS, that will reparameterize the system based on expected energy demand.

2. Introducing optimization algorithm that will be integrated into digital twin to optimally control the power system.

3. Identifying key information needed from the power system to effectively control the system from a digital twin.

1.2 Thesis Structure

This thesis is laid out into six main chapters: The first chapter serves as an introduction to the context of the research, as well as an overview of the research goals. The second chapter provides an overview of the topics presented in this thesis, including DC power systems, digital twin modeling, lithium-ion batteries, and optimization. The third chapter introduces the power system model used in later chapters. Chapter 4 builds the energy storage operating strategies that can be used by a smart system to tailor performance to the situation. The fifth chapter introduces the optimization algorithm developed during this work, as well as emphasizing the necessary

information needed from the power system. The sixth and final chapter presents future studies and improvements for this topic that are in development.

Chapter 2

Background Literature

This chapter presents an overview of the literature motivating this thesis. First, an overview of digital twins and their uses in industry is presented, including two notable uses in the realm of power systems. Next, DC power systems and their potential benefits over AC systems are discussed, inspiring the selection to model a DC power system for the research presented. A discussion of batteries follows, limited to the relevant topics of degradation prompting choices within this thesis. Finally, a brief introduction to power flow optimization is given, highlighting the various methods that can be used.

2.1 Digital Twin Modeling

According to Schluse et al, "digital twins represent real objects or subjects with their data, functions, and communication capabilities in the digital world" [10]. Oracle purports the main benefits of a digital twin system to lie in visibility of large systems, predictive capabilities, hypothetical simulations, documentation, and connection between disparate systems [11]. Digital twins can be applied in a variety of ways and are used in many industries, including health, meteorology, manufacturing and process technology, education, cities, transportation, energy, automotive, aerospace, construction, entertainment, and cybersecurity [12, 13, 14, 15, 16, 17, 18, 19]. The U.S. Naval Sea Systems Command (NAVSEA) has envisioned a digital fleet to model the performance of individual ships, including structural loads and energy consumption, to enhance operational effectiveness and availability and perform condition-based main-

tenance [20]. The Naval Surface Warfare Center in California currently uses a digital twin of the research vessel *Independence* to improve maintenance of the ship [21]. From these disparate uses, it is apparent that there is heavy interest in developing digital twins to handle, interpret, and report on data from systems that are present in all aspects of modern life.

Within the context of power systems, Siemens touts digital twins to increase efficiency and optimize processes, improve accuracy and consistency of network models, integrate transmission and distribution modeling analysis, and provide a foundation for advanced benefits and future digitalization use cases [22]. The digital twin for Fingrid, Finland's transmission system operator, offers a model up to 100 times more detailed than previous models developed manually by engineers [23]. This digital twin model allows for the measured 99.9996 % reliability of the power grid. Additionally, an online analysis digital twin is under development for the Chinese power grid [24, 25, 26, 27]. This model was deployed on the Chinese grid and could track the performance of the over forty thousand bus system with a subsecond delay. Beyond the power system management, it also integrates cybersecurity protocols to help protect the grid. The benefits of these digital twins from both the Finnish and Chinese grids highlight the potential of developing digital twins for power systems.

The model presented in this work seeks to serve as a foundation for the development of a digital twin for a DC power system. The current work contains only a simulation of the power flow, neglecting the digital representation of the physical grid. However, it seeks to identify the data necessary to pass between the various components and levels of the digital twin in line with the Schluse definition and the benefits of a digital twin listed by Oracle.

2.2 DC Power Systems

Since their proposal in 2002, the concept of microgrids has grown to provide a foundation for the development and improvement of smart grids [28, 29, 30]. Compared to AC power systems, DC systems provide more efficient and more reliable power via a reduced number of power converters, reduction of transmission losses by eliminating the AC skin effect, reduction of reactive power, and integration of energy storage [31]. This improvement in efficiency and reliability motivates the usage of DC systems in data centers [32]. Beyond this, DC systems avoid the issues of harmonics, unbalanced systems, synchronization, and reactive power flows that occur in AC systems [33]. Because many modern loads, renewable energy sources, and energy storage systems operate with DC power, either natively in a DC system or after a AC-DC rectifier in an AC system, DC power systems align with present needs [34] and can provide energy savings by utilizing both DC distribution and DC loads [35].

Because microgrids are able to operate in an island mode [36], an ideal candidate for DC microgrid implementation is a shipboard power system. Initial discussions regarding electric ships focused on electric propulsion using DC systems, but an AC system was selected due to high current densities and temperatures [37]. However, the current trend in integrated power systems (IPS) has turned towards using DC systems [38, 39, 8]. The U.S. Navy Office of Electric ships listed the implementation of DC power systems as a recommendation in the Naval power systems technology roadmap [40]. Chang et al. demonstrates the benefits of a DC power system in a marine context, in which a ship outfitted with a fully DC power system outperforms the same ship outfitted with an AC power system [41].

Based on the advantages of a DC power system and the apparent trajectory of both terrestrial and marine power system, this work focuses on a DC system. Serving as a foundational model on power flow, this work ignores some disadvantages brought

about by the use of a DC system, particularly those involving specific hardware or load details [29, 39].

2.3 Energy Storage

Due to differences in chemical and physical make-up of various energy storage devices, background on all possibilities provides too many options and too few details. For the context of this work, research is focused on lithium-based batteries due to their high volumetric and gravimetric energy densities [42]. This limits the scope of work to more specific bounds that allow for significant decisions to be made. Although this work features non-real batteries that are considered ideal, this background informs the decisions of the configuration of the energy storage within the system.

Smith et al. find that the two of the main factors in degradation are charge cycling and state of charge as a function of time [43]. Typical depth-of-discharge experimentation focuses on discharging a fully charged battery and then recharging. These studies find that increasing the depth-of-discharge of a fully charged battery decreases the overall lifetime of the battery [44, 45]. De Vries et al. demonstrate that the number of charging cycles is maximized when the battery is cycled around 50 % [46]. It is shown that the lifetime of batteries is reduced when a high state of charge is maintained [47, 48].

2.4 Power Flow Optimization

Optimal power flow is an important function of any power system, providing a minimum cost to satisfy the constraints of the system [49]. The optimal power flow problem is extensively studied and has a wide range of proposed solutions, including linear programming, Newton-Raphson, quadratic programming, nonlinear programming, Lagrange relaxation, interior point methods, artificial intelligence, artificial neural network, fuzzy logic, genetic algorithm, evolutionary programming, and par-

ticle swarm optimization [50, 51, 52, 53, 54, 55, 56]. One approach to power flow optimization is presented in [57], which aims to maximize the use of distributed energy resources to reduce cost and volatility in the system. This work focuses on the optimization of setpoints for power sources and linearizing the power system parameters, allowing for the use of linear optimization. Linear optimization is less complex than other optimization methods, reducing the magnitude of computational delays necessary to perform the optimization. This reduction is vital to real-time control, as discussed in [58]. The reduction in scope also allows for inclusion of mechanical factors into the electrical optimization due to the decreased computational effort of the optimization function itself.

Due to the benefits of digital twins discussed above, there is interest in developing digital twins of power systems. By developing the system to utilize DC power, the system can capitalize on the increased efficiency and reliability that DC power offers over AC power. A DC system also enables better integration of distributed energy resources, including renewable energy generation and increased prevalence of energy storage. However, it is necessary to develop a model of the power system before development of a digital twin system can continue. The following chapter discussed two iterations of a model of a DC power system developed in this work as part of the development of a digital twin.

Chapter 3

Methodology and Modeling

Before development of the optimization and digital twin can begin, it is necessary to develop a model of the system. This model can be used to determine the parameters of the system and to develop performance metrics. These provide a baseline against which the effects of any future work can be tested.

3.1 Methodology

This section discusses the general concepts that form the groundwork of the work presented in this thesis and in a previously published work by the author [59]. First, the rules used to generate the load profiles with which the power system is tested are introduced. These rules stem from the parameters of the system, generators, and energy storage devices. Next, there is a brief discussion of the motivations while developing the energy storage. Finally, the metric of total load service is presented, forming the basis for the testing of the power system model.

3.1.1 System Parameters and Load Profiles

Adapting the single-bus system presented in [60], the modeled system contains two main turbine generators (MTGs), each with a maximum power capacity of 35 MW and a ramp rate of ± 1 MW/s, and two auxiliary turbine generators (ATGs), each with a maximum power capacity of 6 MW and a ramp rate of ± 1.5 MW/s. The system also contains four batteries in the energy storage (ES) system, each with a maximum energy capacity of 60 MJ and a power rating of 10 MW. Each battery is assumed

to be 100 % efficient. This is an unrealistic assumption for both the battery and its system-interfacing converter, but the current model simplifies the ES to focus on the generation. As such, the system is capable of producing a maximum of 122 MW of power. The load profiles generated for testing in this work use 120 MW as the upper bound of demand. These parameters are summarized in Table 3.1.

Table 3.1 Power System Parameters

Parameter	Value
MTG Max Power	35 MW
ATG Max Power	6 MW
MTG Ramp Rate	±1 MW/s
ATG Ramp Rate	±1.5 MW/s
Storage Power	10 MW
Storage Energy	60 MJ
Storage Efficiency	100 %

The ramp rates of the load profiles were approximated using the generation ramp rates. It was assumed that the load ramp rate does not exceed the MTG max ramp rate, so that one operational MTG can provide power during the transition period of the normal load changes. This means that the general load ramp rate is limited to ±1 MW/s. During the pulse load events, a step response was approximated with a ±20 MW/s ramp rate, vastly exceeding the MTG capability.

Additional constraints were placed on the load profiles to ensure more uniform behavior despite the random generation. For the general load, eight to twelve transitions, segments of the profile where the general load transitions from one steady state value to another, were allowed to provide a variety of cases in which the number of transitions might affect the result. Each general load transition had to complete before another transition could occur due to the additive nature of the model. Impulse loads were limited to twelve occurrences and grouped in clusters of up to three pulses. Each pulse consists of 1 s rise time, 1 s period at maximum power, a 1 s fall time, and

1 s between pulses for repetitive pulses. Ten load profiles were developed for testing the model configurations presented in this work, shown in Fig. 3.1.

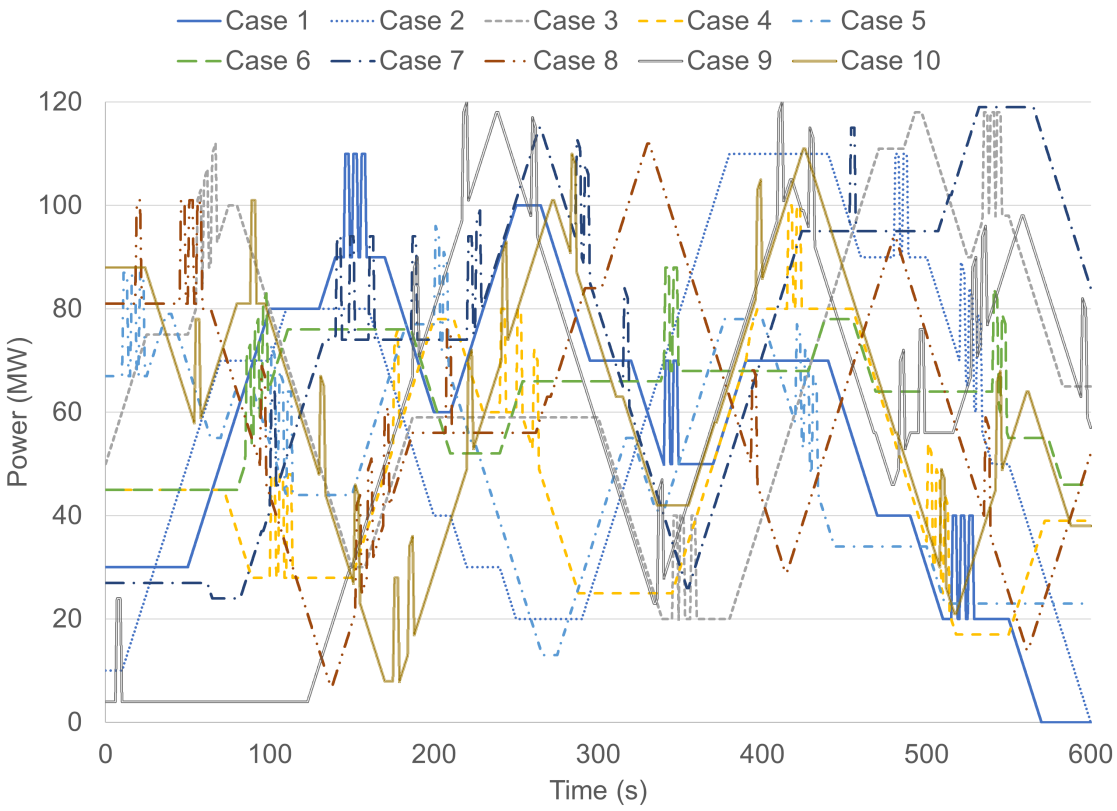

Figure 3.1 Ten load profiles, meeting the prescribed requirements, used in various studies for this work.

3.1.2 Energy Storage Management

In a power system with integrated energy storage, it becomes necessary to control how the energy storage behaves. Both models presented are configured so that the energy storage only discharges if the load demand is greater than the generator output. To maintain a sufficient energy reservoir, a charging protocol for the energy storage system is required. Each version utilizes a rules-based method to determine the generator outputs used to recharge the energy storage.

3.1.3 System Performance

All performance metrics in this work are defined in terms of unserviced load and Total Load Service (TLS). Unserviced load is the quantity of load in excess of the system capabilities at any specific time by which the load must be reduced to feasibly operate the system. In this work, unserviced load has no effect on the function of the system beyond a metric. Unserviced load is measured both graphically, showing both magnitude and duration of instances where there is load in excess of generation capabilities, and quantitatively by measuring the energy represented by this graphical representation. This energy is reported as both a raw quantity and as a percentage of the total load energy of the profile.

TLS is defined as servicing 100 % of the load throughout the runtime of the load profile test. This qualification was chosen arbitrarily, but represents the most strict metric of the system. As such, the performance of the system represents a worst case scenario where there is no margin of success and the entirety of the load must be serviced throughout the test.

3.2 Lumped-Generation Model

This section presents a model that serves as a baseline for performance and uses a cascaded distribution method to set the operating point of the generators and the energy storage. It considers all generators to act as one unit and all energy storage to act as one unit. It also features a static rules-based method to recharge the energy storage. This is featured in previously published work [59].

3.2.1 Lumped-Generation Model Configuration

The lumped-generation model is configured as a simplified single bus system. While it has two MTGs and two ATGs, as defined in Table 3.1, these four generators are considered to be one unit. As such, the power capacity and ramp rate of this single-

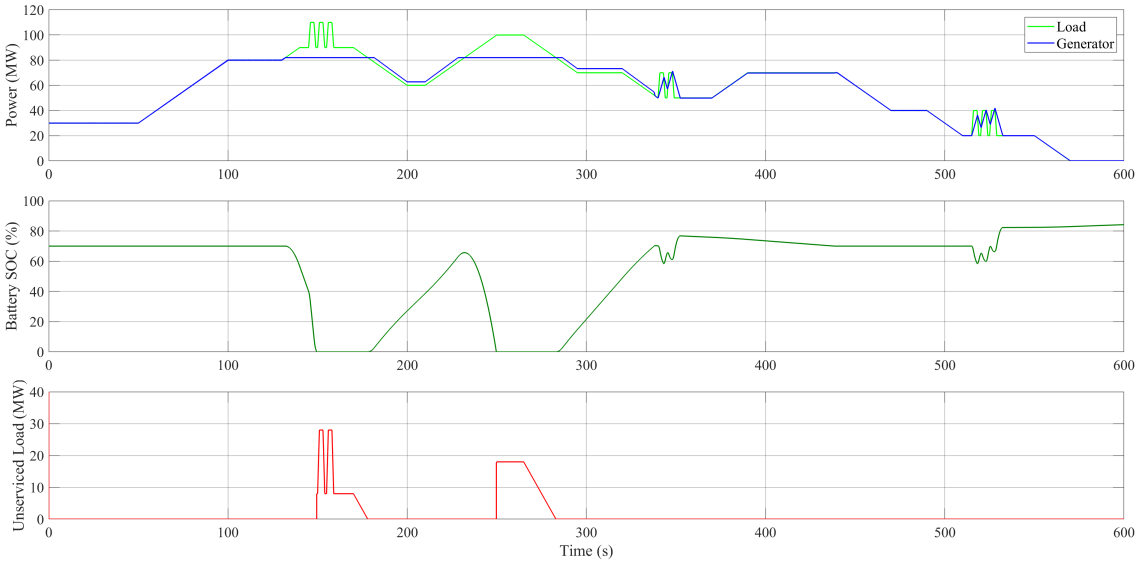

Figure 3.2 Case 1 load profile tested in the lumped generation model. First plot: generation vs load. Second plot: energy storage. Third plot: unserviced load.

point generation are 82 MW and ±5 MW/s. Likewise, the four energy storage devices are considered to be another single point on the bus, resulting in a total power of 40 MW and a total energy capacity of 240 MJ.

The system is organized as a cascaded system such that the load demand from the load profile is satisfied as much as possible by the generator, then by the energy storage, and the excess load is marked as unserviced load. The system is also configured such that, if the generator output is greater than the load demand, the excess power is used to recharge the energy storage. This configuration uses a static scaling method to adjust the output of the generator if the current state of charge is below a target threshold. This causes the generator to perceive a load that is 5 % larger than the actual load demand, creating excess power that is used to recharge the energy storage. Because the generator needs time to ramp down, the target state of charge must be low enough to allow for charging past the target while being high enough to provide sufficient storage. This target was chosen to be 70 %.

The key performance features of this model version can be seen in Figure 3.2. This figure shows the load demand versus the generator output in the top plot, the state of charge in the middle plot, and the quantity of unserviced load, as defined in Section 3.1.3, in the bottom plot. In terms of generation, it can be seen that the maximum generation capacity is 82 MW as the generator trace in the top plot plateaus at this value in the time frames around 150 s and 250 s. The ramp rate of ± 5 MW/s can be seen during the pulse clusters around 350 s and 525 s. The offset between the load and the generator traces apparent at 300 s highlights the recharge protocol described above. In terms of energy storage, the initial plateau at 70 % shows the target state of charge setting. By converting the state of charge to an energy capacity value and measuring the rate of change, the power use of the energy storage is confirmed to be less than or equal to 40 MW throughout the simulation.

3.2.2 Lumped-Generation Model Results

Only Cases 4-6 pass the evaluation of TLS, as discussed in Subsection 3.1.3, presented in this work. Each of the other cases have a non-zero percentage of the load demand that is unserviced, varying from 2.21 % to 10.63 %. Figure 3.2 shows the results of the evaluation for Case 1 and Table 3.2 shows the results of all ten load profiles tested in this work. The table shows the total energy demanded by the load and the energy of the unserviced load, as both quantities of raw energy and as a percentage of the total load energy.

As can be seen in Figure 3.2, the primary cause of failure in terms of TLS is a period of time during which the load demand exceeds the capacity of the generator. Because energy is the time integral of power, both the magnitude of the load demand and the time that it exceeds the generator capability affect the quantity of energy needs that will not be met. This energy deficit is further exacerbated if there is a

Table 3.2 Lumped-Generation Model Results

Case	Total Load Energy (kWh)	Unserviced Load Energy (kWh)	Unserviced Load (%)
1	9438.89	208.97	2.21
2	10305.56	760.00	7.37
3	11050.00	766.39	6.94
4	7783.33	0.00	0.00
5	8088.89	0.00	0.00
6	10536.11	0.00	0.00
7	12349.99	1313.06	10.63
8	10030.52	225.47	2.25
9	9311.11	542.78	5.83
10	10297.18	290.28	2.82

coincidence of high load demand with pulse loads. This trend holds for all profiles tested.

Case 1 features two instances of TLS failure. Both instances feature a baseline load that exceeds the generator capability. The first period of failure occurs during a 46 s period where the load demand exceeds 82 MW capabilities of the generator and there are three load pulses. This period demands 134.45 kWh, while the energy storage has 46.67 kWh stored. This difference causes the failure in load service during the period of 150 s to 178 s. The second point of failure occurs between 250 s and 283 s. This occurs during a 51 s period where the load exceeds the generation capability, reaching a peak of 100 MW. This period demands 165.01 kWh from the 43.79 kWh available in the energy storage.

3.3 Distributed Resource Model

This section introduces a model that uses a proportional distribution method to allocate a portion of the load to each of the generators and energy storage devices. Each generator and energy storage device is treated as an individual unit in the system. The energy storage recharge method is more dynamic than that in Section 3.2.

3.3.1 Distributed Resource Configuration

The distributed resource model is also configured as a single bus system. Unlike the lumped-generation model, each generator and energy storage device is treated as a discrete component and is accounted for separately, using the parameters defined in Table 3.1. Instead of treating the load as a single quantity, it is distributed proportionally across the four generators and, in the event of use, the four energy storage devices. This distribution is intended to be replaced by the optimization model discussed in Chapter 5.

Like the lumped-generation model, the energy storage subsystem is configured such that it is unused if the load demanded does not exceed the capabilities of the generators alone. Should the load demand be less than the current output of the generators, the excess power is routed towards the energy storage to recharge that system. Instead of the more passive and static recharging protocol in the baseline model, the distributed resource model adjusts the set-point of the generators relative to the difference between the current and desired states of charge of the energy storage. This means that, if the difference is 50 %, the generator control is configured to increase the output by 50 % of the maximum output of the generator. Because the difference reduces to 0 % as the energy storage recharges, the generator does not need to ramp down after the charging protocol is complete. Thus, the chance of overcharging the energy storage is greatly reduced and the target state of charge can be set to 100 %.

The key features of the distributed resources model configuration can be seen in Figure 3.3. This figure shows the load demand versus the four generator outputs in the top plot, the state of charge of the four energy storage devices in the middle plot, and the quantity of unserviced load, as defined in Subsection 3.1.3, in the bottom plot. In terms of generation, it can be seen that the maximum capacity of the MTGs is 35 MW, and that of the ATGs is 6 MW. The maximum power of the

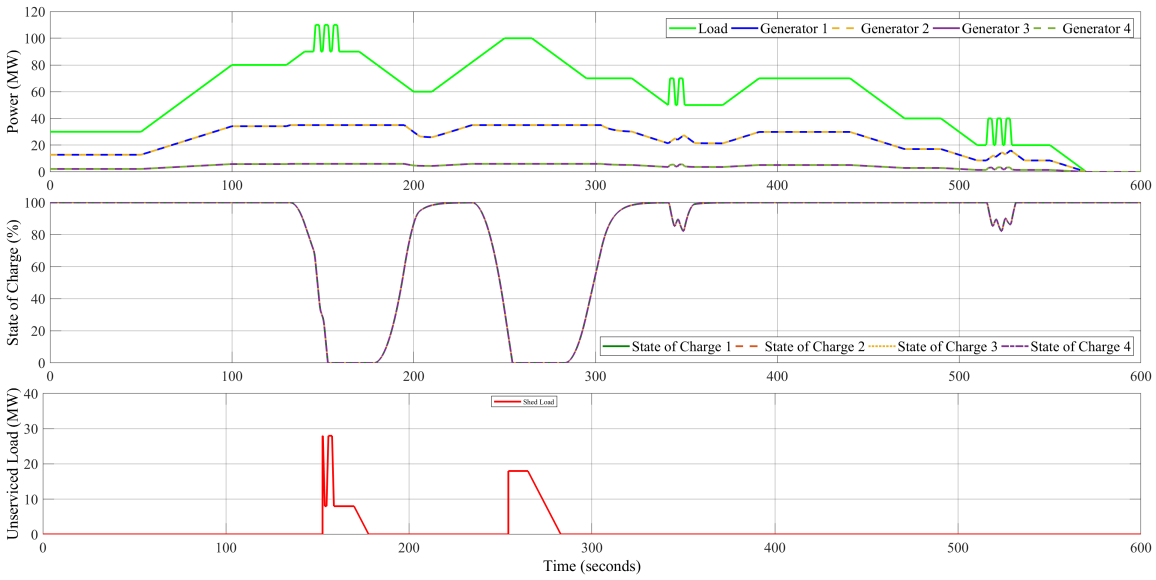

Figure 3.3 Case 1 load profile tested in the distributed resource model. First plot: generation vs load. Second plot: energy storage. Third plot: unserviced load.

generators can be seen in the time frames around 150 s and 250 s when the generators are unable to increase their outputs. The MTG ramp rate of ± 1 MW/s can be seen during the pulse clusters around 350 s and 525 s. However, the ATG ramp rate of ± 1.5 MW/s, while present at the same time, is harder to see in this image due to the small magnitude change. In terms of energy storage, the initial plateau at 100 %, as well as the return to full charge, shows the target state of charge setting. When compared to recharging periods in Figure 3.2, the energy storage in the distributed resource model shows a more polynomial curve, reflecting the design that the charging protocol becomes less intensive as it reaches completion. By converting the state of charge to an energy capacity value and measuring the rate of change, the power use of the energy storage is confirmed to be less than or equal to 10 MW for each energy storage device throughout the simulation.

3.3.2 Distributed Resource Configuration Results

Like in the lumped-generation model, only Cases 4-6 pass the evaluation of TLS. Each of the other cases have a non-zero percentage of unserviced load demand, varying from 1.76 % to 10.19 %. Figure 3.3 shows the results of the evaluation for Case 1, and Table 3.3 shows the results of all ten load profiles tested in this work. The table shows the total energy demanded by the load and the energy of the unserviced load, as both quantities of raw energy and as a percentage of the total load energy.

Table 3.3 Distributed Resource Model Results

Case	Total Load Energy (kWh)	Unserviced Load Energy (kWh)	Unserviced Load (%)
1	9438.89	166.06	1.76
2	10305.56	740.00	7.18
3	11050.00	722.22	6.54
4	7783.33	0.00	0.00
5	8088.89	0.00	0.00
6	10536.11	0.00	0.00
7	12349.99	1258.06	10.19
8	10030.52	197.19	1.97
9	9311.11	487.22	5.23
10	10297.18	251.58	2.44

As discussed in Subsection 3.2.2, the primary cause of failure through all the profiles remains periods of time where the load demand exceeds the generation capability. Notably, overall performance of the distributed resource model is better than that of the lumped-generation model. This is due to the target state of charge being larger because the chance of overcharging is reduced with the dynamic charging protocol, providing a larger reservoir. Additionally, the dynamic charging protocol leads to faster recharging at low states of charge, so there is more likely to be stored energy in the event of rapid switching of the load.

3.4 Modeling Conclusions and Future Works

This chapter has presented two versions of a model for a DC power system. As shown, the two models are capable of servicing the generated load profiles, albeit to different extents. From the ten randomly generated profiles, three allow for total load service with the given parameters. Amongst the other seven, there were commonalities to the points where there is a non-zero quantity of load that is unserviceable. The principal indicator that a load profile would fail the total load service criterion was an extended duration during which the magnitude of the load exceeded the capabilities of the generators. The length of time that would cause the evaluation to fail depends on the extent that the load exceeds the generation capability, with a larger load requiring a shorter time before depleting the energy storage. This is exacerbated by the coincidence of pulsed loads with loads above the 82 MW that the combined capabilities of the generators. These instances of unserviced load demand indicate the factors of the model that cause failure of total load service, as well as a comparison for results of the works presented later in this thesis.

While the distributed resources model provides the basis for the further works in this thesis, there is future work needed to develop the model. There are two main avenues for this development: load definition and hardware modeling. In this work, the load is an abstracted quantity of energy demand used to evaluate the performance of the model. As mentioned in Section 3.1.3, total load service was the chosen criterion because it represents the worst case scenario for the system where the load must be serviced at all times. By defining the loads by type, magnitude, and priority, it will be possible to create a methodology to shed the unserviceable load quantity to reduce the load to the level that it is serviceable. With definitions for load priority, the load shedding protocol can shed loads that are not vital to the operation of the system. Along the same lines, the model treats the system as a purely mathematical concept, having ideal sourcing, transmission, and loading. In future models for the

development of a digital twin, it is necessary to model the non-idealities of the system. In particular, this involves modeling the components that comprise the system. This hardware will introduce losses into the system for which the model must account to make it more accurate.

Chapter 4

Energy Storage Operating Strategies

Although the load profiles tested in this work all follow the same rules in construction, a real system will experience much more variety in loading conditions. Many power grids feature regular times of high demand throughout their operating cycle [61]. Using the codified relation between situation and resource-use of the US Navy conditions of readiness [62] as a inspiration, this work develops two energy storage operating strategies (ESOSs) to emulate the change in need between different scenarios that a power system may encounter.

This work considers a simplified framework of a system of ESOSs, in which one strategy prioritizes system health and the other prioritizes system performance. In the health-priority energy storage operating strategy (HP-ESOS), the goal of the system is to provide power to the system while minimizing the effects of degradation on the energy storage devices. This strategy can also be used when there is generally low demand or for periods where high demand or high impulse loads follow a predictable routine, allowing for preparation. Alternatively, it may be beneficial to adopt a performance-priority energy storage operating strategy (PP-ESOS) and trade decreased system health for increased performance in the short term. This could occur during periods of generally high load demand or during periods where there is the potential for many high impulse loads that are vital to the system operation.

4.1 Energy Storage Operating Strategies Configuration

In general, the two ESOSs use the same parameters. The PP-ESOS uses the parameters defined in Subsection 3.3.1. The major difference between the two ESOSs is the target state of charge. The energy storage in the PP-ESOS is recharged to full capacity. In the HP-ESOS, the energy storage recharges to a state of charge that is less than 100 %. For this study, the target was set to 50 %. This target level can be seen in Figure 4.1.

The reason for this reduction is twofold. First, in the HP-ESOS, the stored energy is assumed to be less necessary to the system performance, so less capacity is needed. This also allows for reallocation of energy between the storage devices should maintenance be required. The second reason is for the health of the energy storage devices. De Vries et al. find that partial state of charge cycling around 50 % offers the longest lifespan for lithium-based batteries [46]. It was also chosen to allow the state of charge to exceed 50 % without discharging to meet the target, as discharging would cycle more charge, which Smith et al. find to be one of the primary causes of battery degradation. Also within system health considerations, energy storage left at full charge will degrade faster than that left at a lower state of charge [43]. In this model, the target state of charge is configurable, such that different battery chemistries could be simulated.

4.2 Energy Storage Operating Strategies Results

Almost universally, except in the cases that pass the TLS criterion, the load profile tests using the HP-ESOS perform worse in terms of unserviced load than the tests conducted with the PP-ESOS. This is consistent with the reduction in energy stored throughout the simulation, as a reduction in supply with the same demand will result in an increase in the amount of deficit. The results are shown in Table 4.1.

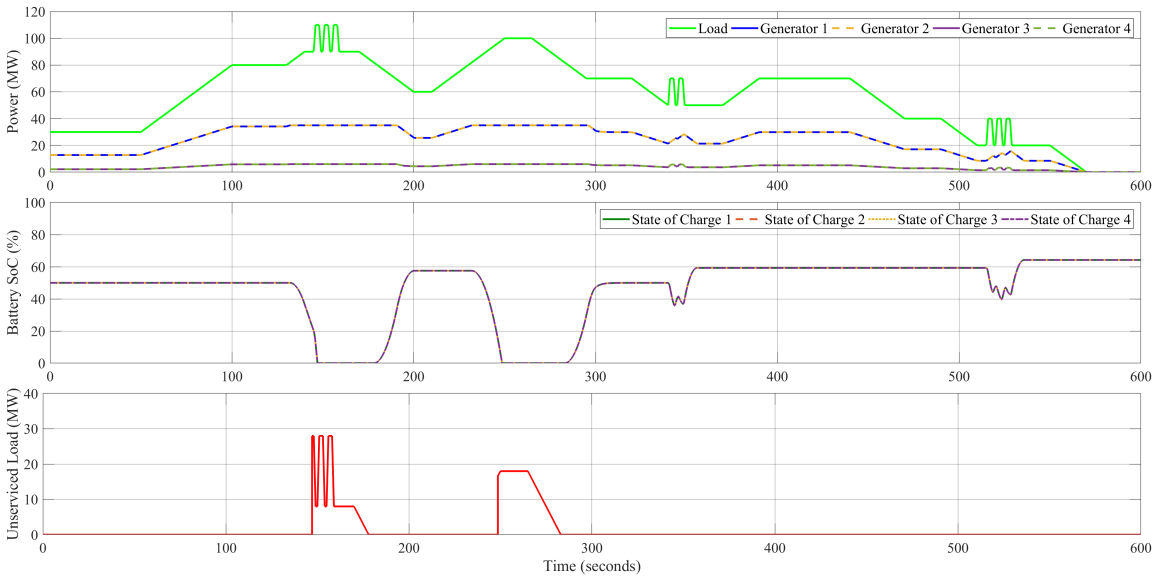

Figure 4.1 Case 1 load profile tested in the HP-ESOS. First plot: generation vs load. Second plot: energy storage. Third plot: unserviced load.

Examining Case 1, shown in the PP-ESOS in Figure 3.3 and in the HP-ESOS in Figure 4.1, it can be seen that the energy of the unserviced load is 166.06 kWh and 232.75 kWh in the PP- and HP-ESOSs, respectively. Both ESOSs result in TLS failures in the same regions of the load profile, but the duration of failure is extended in the HP-ESOS. This is most notable in the additional pulse and a half of unserviced load demand in the HP-ESOS.

4.3 Changing Energy Storage Operating Strategies

A benefit of having the different strategies established is that the system can shift between ESOSs according to established protocols. For instance, a change can be triggered so that the system shifts from a HP-ESOS to a PP-ESOS to increase the target state of charge of the energy storage in preparation for the load increase if the system expects an increased likelihood of the need for stored energy. In this work, the transition follows a simple protocol of changing the ESOS halfway through the simulation. However, additional rules could be implemented in the model easily.

Table 4.1 Health-Priority Energy Storage Operating Strategy Results

Case	Total Load Energy (kWh)	Unserviced Load Energy (kWh)	Unserviced Load (%)
1	9438.89	232.75	2.47
2	10305.56	773.33	7.50
3	11050.00	793.33	7.18
4	7783.33	0.00	0.00
5	8088.89	0.00	0.00
6	10536.11	0.00	0.00
7	12349.99	1340.28	10.85
8	10030.52	262.14	2.61
9	9311.11	587.22	6.31
10	10297.18	330.00	3.20

The change from the HP-ESOS to the PP-ESOS and vice versa can be seen in Figures 4.2 and 4.3, respectively. These figures both show the Case 8 load profile. As can be seen, the target states of charge switch between 50 % for the HP-ESOS and 100 % for the PP-ESOS at 300 s.

When comparing the two figures visually, the performance difference is evident. There are three instances of TLS failure that are marked by the non-zero portions of the unserviced load plots in Figures 4.2 and 4.3. The period of unserviced load around the 60 s mark of Figure 4.2 is caused by pulse loads rapidly depleting the stored energy. However, the same pulse loads are able to be serviced in their entirety in the change from the PP-ESOS to the HP-ESOS because there is a greater amount of energy initially stored in the PP-ESOS. The lack of unserviced load can be seen in Figure 4.3 around the same 60 s mark. Another TLS failure occurs when changing from the PP-ESOS to the HP-ESOS, around 490 s in Figure 4.3. This small spike of unserviced load is caused by the depletion of the energy storage by the load peak above 80 MW. In the change from the HP-ESOS to the PP-ESOS, there is enough stored energy during the second half of the simulation to provide the necessary energy.

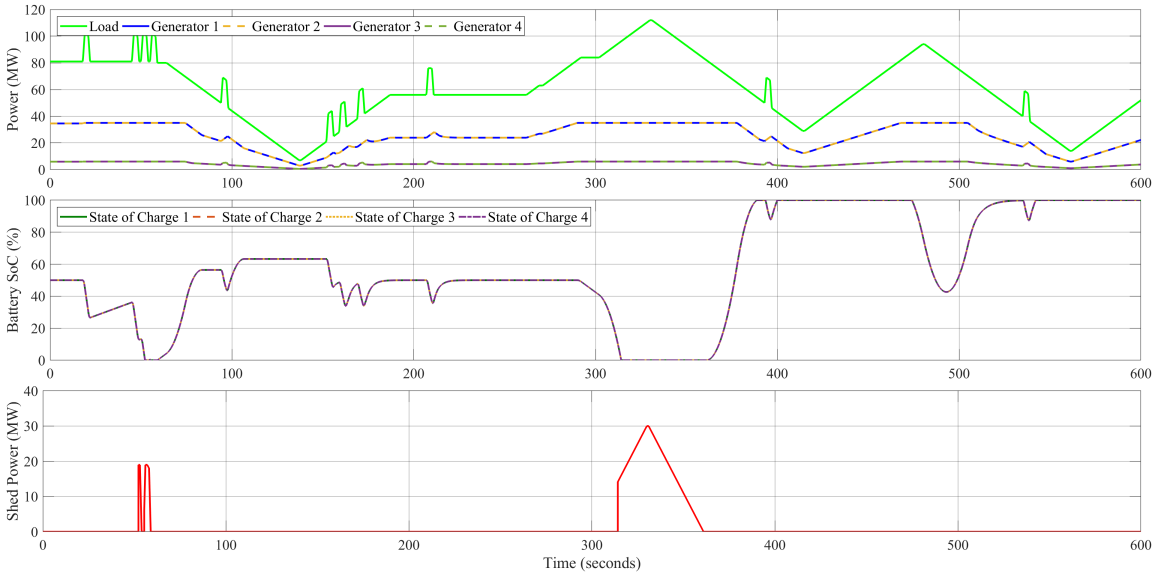

Figure 4.2 Case 8 changing from the HP-ESOS to the PP-ESOS. First plot: generation vs load. Second plot: energy storage. Third plot: unserviced load.

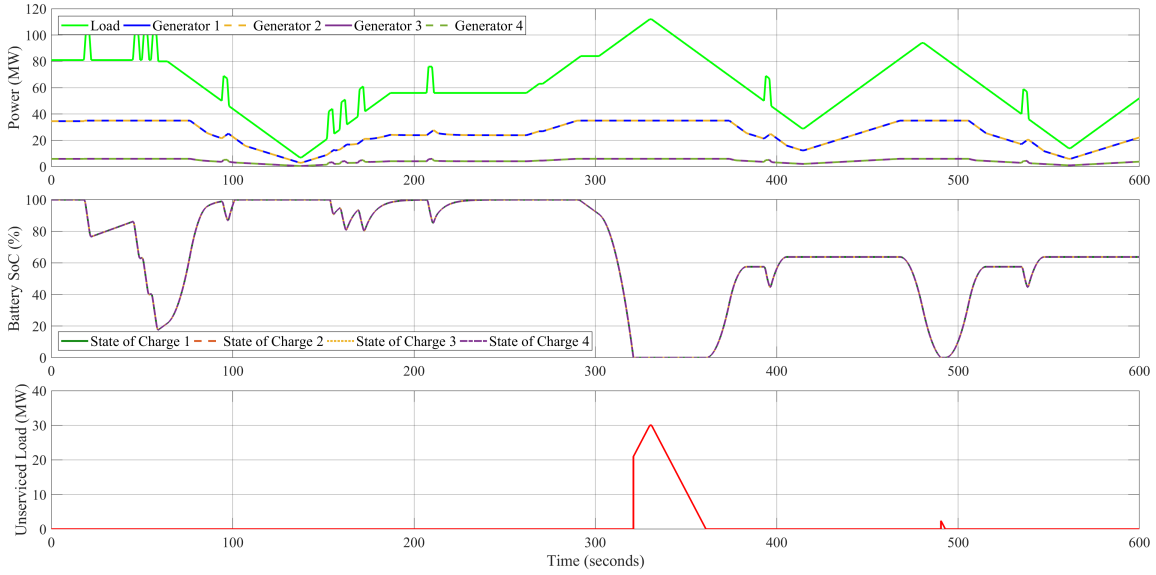

Figure 4.3 Case 8 changing from PP-ESOS to the HP-ESOS. First plot: generation vs load. Second plot: energy storage. Third plot: unserviced load.

Table 4.2 Energy Storage Operating Strategies Change Results

Case	HP- to PP-ESOS Unserviced Load (%)	PP- to HP-ESOS Unserviced Load (%)
1	2.41	1.76
2	7.18	7.18
3	6.84	6.65
4	0.00	0.00
5	0.00	0.00
6	0.00	0.00
7	10.46	10.41
8	2.51	1.97
9	5.57	5.70
10	2.88	2.72

The TLS failure around 325 s is the most interesting result. It is a common instance of failure between the simulations changing the ESOS, so it is unavoidable as far as the capabilities of the system. However, the magnitude of energy that is unserviceable represented in the point of failure depends on the previous ESOS. In either case, the period of unserviced load demand begins in the first ESOS and extends though the change to the second ESOS. In the change from the HP-ESOS to the PP-ESOS, the state of charge at that time is around 50 %, as expected in the HP-ESOS. Due to the lower state of charge, the load demand depletes the energy storage more quickly, causing a longer duration of unserviced load. In the change from the PP-ESOS to the HP-ESOS, the energy storage is initially at 100 %, providing roughly twice as much energy before depletion. This results in an instance of TLS failure that is reduced in duration than in the change from the HP-ESOS to the PP-ESOS. The results for the two ESOS change simulations are shown in Table 4.2 in terms of the quantity of the percentage of load energy that is not serviceable.

The results of the HP-ESOS, the PP-ESOS, the change from the HP-ESOS to the PP-ESOS, and the change from the PP-ESOS to the HP-ESOS evaluations are shown in Figure 4.4 in terms of percentage of load energy that is unserviceable. As

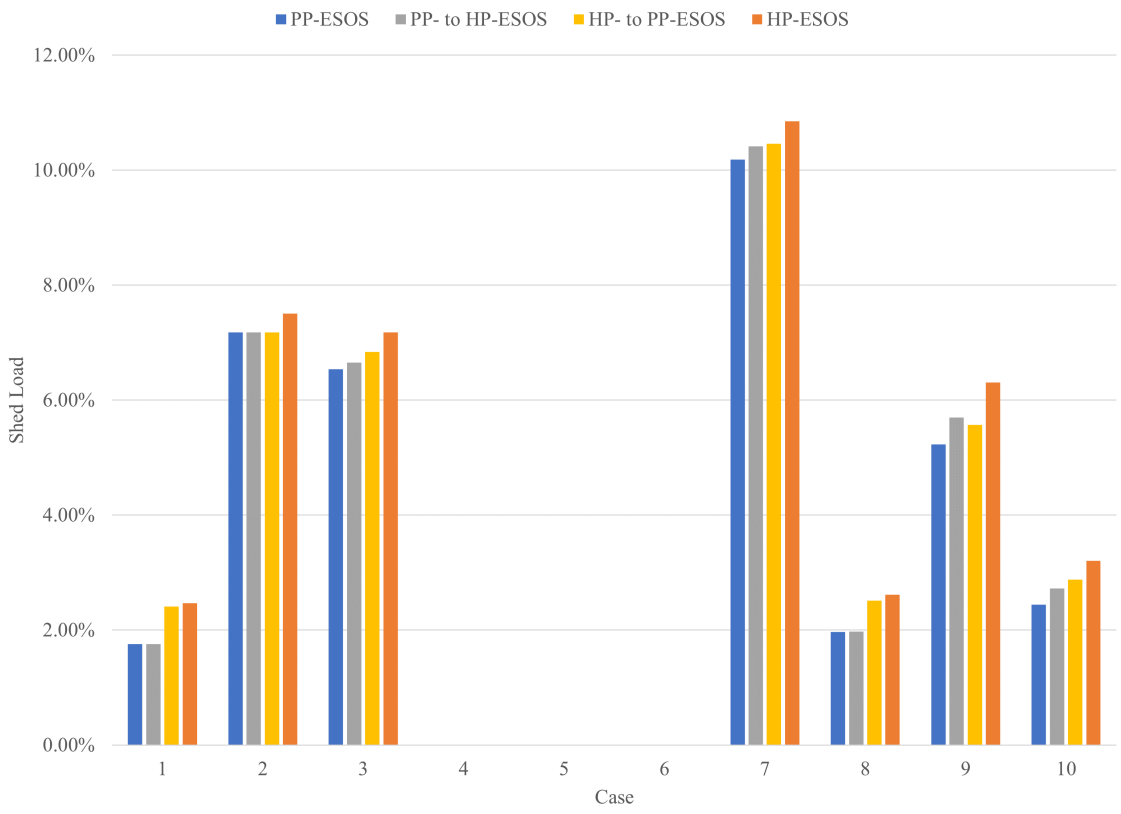

Figure 4.4 ESOS and ESOS-change result comparison. Results reported in percent of energy that is unserviceable throughout the simulation.

seen in this comparison, the HP-ESOS and the PP-ESOS are at the extremes of the performance with all seven non-TLS cases performing the best in the PP-ESOS and the worst in the HP-ESOS. As expected, the ESOS change simulations usually perform in between these two extremes. In some cases, the change results can match those of one of the pure ESOS simulations if the points of failure occur in one half of the simulation such that only one ESOSs parameters are relevant to the amount of unserviced load.

4.4 ESOS Conclusions and Future Works

As stated in Section 1.1, a main goal of the research presented in this work is to develop a strategies to manage the energy storage in the system by redefining parameters of the system. This section presents two energy storage operating strategies that redefine the target state of charge levels for the energy storage in order to prioritize the performance or the health of the system. As shown in Tables 3.3 and 4.1 and Figure 4.4, there is an apparent trade-off between the performance of the system, measured by the quantity of unserviced load demand, and the health of the energy storage, abstracted by the relationship between battery longevity, state of charge, and amount of charge cycling. The evaluation also verifies that changing the ESOS results in performance between the extremes of the two strategies. This work accomplishes the goal of implementing basic energy storage operating strategies.

To further develop this concept, future works will focus on developing more granular ESOSs and and rules-based implementation of ESOS changes. The ESOSs in this work exist as a binary state, where the system is either prioritizing the health or performance of the system. More granular definitions can fill in the spectrum between health-priority and performance-priority. This will allow for a more optimal trade-off between health and performance depending on the demands of the situation. This will also be aided by developing rules to automate ESOS changes. Because there is a relationship between the magnitude of the load and likelihood that there will be unserviced load demand, an automated rule may be able to preemptively reparameterize the system based on the probability of unserviceable load. This may not be desired at all times, so an operator should always be able to override the system automation.

Chapter 5

Optimization and Key Information

Instead of the proportional allocation of power from the generators and the energy storage to the load, as in Section 3.3, the final system will rely on an optimization algorithm to determine the set-points of the generators and energy storage. The following chapter introduces the initial optimization algorithm. It currently functions on steady-state load values and is intended to be used on the system with the HP-ESOS. The limit to steady-state values is because the non-changing values are easier to implement as a first step rather than having to also account for the linear change in load through time. As for the ESOS, this initial optimization function was assumed to prioritize system health and the optimization function is developed with this in mind. This work builds on the optimization section presented by the author in an earlier publication [59].

5.1 Optimization Definition

Using the parameters from Table 3.1, the power system is defined with $N = 4$ generators and $M = 4$ energy storage devices. Each generator has a particular maximum power output, described as P_j where j identifies the corresponding generator, $j = 1$ and $j = 2$ for the MTGs and $j = 3$ and $j = 4$ for the ATGs. Likewise, each energy storage device can be described as P_i. At any moment, the power utilization of a generator can be described as $\alpha_j P_j$, where α_j is the percent utilization of the generator where $0 \leq \alpha_j \leq 1$. Correspondingly, the energy storage utilization can be described as $\beta_i P_i$, where β_i is the percent utilization of the energy storage. However, the range

on β_i is $-1 \leq \beta_i \leq 1$ due to the ability of the energy storage to be a load or source device. The generator and energy storage outputs are summed with the intention of satisfying a load, P_L, with the possibility of unserviced load, P_{excess}, as discussed in Chapter 3. This leads to a relationship of

$$\sum_{j=1}^{N} \alpha_j P_j + \sum_{i=1}^{M} \beta_i P_i = P_L + P_{\text{excess}}. \tag{5.1}$$

However, the energy storage has charging and discharging requirements, such as constant current constant voltage charging or pulsed charging methods [63]. These requirements are not currently represented in the constraints of the optimization function and will need to be developed in future work.

Each generator consumes a certain amount of fuel to run, varying as a function of the power output. As fuel is a finite and expensive resource, optimal function of a power system should minimize the fuel consumption to extend the lifetime of a supply and reduce the expense rate of purchasing fuel for the health-focused ESOS. This fuel consumption will be denoted as F_j. The relationship between $\alpha_j P_j$ and F_j varies between generator models, so the optimization function can use the Specific Fuel Consumption, SFC, curves of the generator as a feature to model F_j. This gives rise to a relationship of

$$\alpha_j P_j(SFC_j) = F_j. \tag{5.2}$$

Each generator and energy storage device also produces some amount of thermal energy in the form of heat dissipation due to electrical losses and mechanical friction. This heat is extracted through a thermal bus. Heat can be analyzed using circuit analogy techniques and transferred via a heat exchanger, similar to an electrical bus [64]. Thermal ground is considered the baseline ambient temperature, T_a, of the thermal system prior to any heat removal. The increase in temperature on the thermal bus resulting from each heat generating component is defined as ΔT_k, where k includes all heat generating components. The maximum temperature each heat

generating component thermal bus can reach is $T_{k,m}$. Generator function and safety will be severely impaired if the heat generated exceeds the ability of the thermal bus to extract generated heat. Merging the thermal constraints into matrix form provides

$$T_a + \Delta\mathbf{T} \leq \mathbf{T}_m. \tag{5.3}$$

Component location determines if the thermal bus is for a single component or multiple components, and all thermal buses do not have to be in the same heat exchange loop. Therefore, the physical system design and component location is required to fully represent the thermal aspects of the system.

A key aspect that cannot be neglected is component degradation. For example, an energy storage device can handle a finite number of cycles before it can no longer maintain full capacity utilization. This is dependent on the number of cycles, the charging and discharging time and methodology, and the current used in the charging process. In this function, the energy storage degradation factor is defined as D_i. In a similar manner, the generators also have degradation factors caused by mechanical stresses, including fuel and oil purity, friction, and combustion and rotational stresses. Generator maintenance keeps the generators running smoothly, but they will work less efficiently over time. The generator degradation factor is defined as D_j. A goal of the optimization model is to reduce degradation over time, $\frac{d}{dt}D$, for both the generators and the energy storage.

Merging this information, a linear program is constructed to determine the output of each generator and energy storage device that will minimize fuel consumption and the rate of degradation while satisfying the load and staying within the thermal constraints. This linear program is given in standard form as

$$
\begin{aligned}
\text{minimize} \quad & \sum_{j=1}^{N} F_j + \sum_{j=1}^{N} \frac{d}{dt} D_j + \sum_{1=1}^{M} \frac{d}{dt} D_i \\
\text{subject to} \quad & 0 \leq \alpha_j \leq 1 \\
& -1 \leq \beta_i \leq 1 \\
& \alpha_j P_j(SFC_j) = F_j \\
& \frac{T_a}{T_{k,m}} + \frac{\Delta T_k}{T_{k,m}} - 1 \leq 0 \\
& \sum_{j=1}^{N} (k_1) P_j + \sum_{i=1}^{M} (k_2) P_i + k_3 = 0.
\end{aligned}
\tag{5.4}
$$

Ideally, the power system would be able to provide the power that is demanded by the load. However, as shown in Chapter 3, there are instances where the load demand exceeds the capabilities of the generation and energy storage. For this reason, it was necessary to account for both instances of unserviced load and total load service. The variables of k_x in Equation 5.4 are replaced with the definitions in Equation 5.5, depending on whether there would be total load service or not.

$$
\begin{aligned}
\text{If } P_{\text{excess}} = 0, \quad & k_1 = \tfrac{\alpha_j}{P_L} \\
& k_2 = \tfrac{\beta_i (SoC_i)}{P_L} \\
& k_3 = -1 \\
\text{If } P_{\text{excess}} > 0, \quad & k_1 = \tfrac{\alpha_j - 1}{P_L} \\
& k_2 = \tfrac{(\beta_i - 1)(SoC_i)}{P_L} \\
& k_3 = 0
\end{aligned}
\tag{5.5}
$$

5.2 Optimization Conclusions and Future Works

This chapter has presented the basis of the future optimization work to control the system. Initial testing of the algorithm provides different results for the α and β values, depending on the input of load demand. This fulfills the second research goal of this thesis by introducing an optimization function that can be implemented into a digital twin to control the generator and energy storage set-points more optimally

than the proportional allocation of load that is used by the distributed resources model in Chapter 3. However, further work is needed to develop the algorithm to a functional level that provides meaningful values.

To begin, additional constraints must be created to manage system behavior. Early testing results in setting one generator to maximum output before raising the set-point of the next. While this is may be more efficient in terms of fuel consumption, it is less desirable to start and stop the generators in this way. Additional works are also needed to develop the operation of the optimization algorithm. First, the optimization function defined in this chapter is designed to operate with the HP-ESOS. A new function will be required to control operation in the PP-ESOS, due to the lesser priority of the rate of degradation of components. Next, this function has been designed with the assumption that the load is a constant value. Optimization during the transition states between constant load values will require additional computation. Finally, a method to optimize the pulse loads will be investigated. Because the pulses follow a strict definition for magnitude and duration, it is possible to optimize the system based on the known pulse profile rather than optimizing on a moment-by-moment basis.

5.3 Power System Key Information

The final research goal of this work is to identify key information that is needed from the power system to allow the digital twin to control the system. Based on the values defined in the optimization function, the key information needed at this stage is the present values for load demand, whether the load demand will result in unserviceable load, and the thermal information about the system. To know if the load demand will result in unserviceable load, the set-points of the generators and energy storage must also be known. Future developments in the model and optimization function will require reevaluation of the key information.

Chapter 6

Works in Consideration

This chapter introduces two aspects of the model that can serve as first steps in future works. First, the current state of the model is tested against two disturbance profiles that modify the existing load profiles. While this work does not introduce any methods to mitigate disturbances, the results of evaluating the disturbances provide insight into needed methods. The second aspect is the development of a decision matrix to examine the trade-off between pulse power and the number of pulses before the system energy storage is depleted. This can provide insight for a human operator or as a resource for a digital twin decision maker.

6.1 Disturbance Management

To test the resiliency of the model, it was necessary to apply power disturbances to the load in addition to the normal load profiles. These disturbances were constructed according to the model parameters. The duration and distribution of disturbances are intended to minimize the chances that a disturbance could be applied with limited effect on the performance with various load profiles. This testing was performed on both the HP-ESOS and the PP-ESOS, as discussed in Chapter 4.

To construct the disturbances, a couple parameters were selected to make testing simpler. First, the magnitude of the disturbances was selected to be 10 % of the total generation capability, or 12 MW. This is also equivalent to the combined power output of the two ATGs. Second, the ramp rate of the disturbance was limited to ± 3 MW/s, representing the combined ramp rate of the two ATGs. Third, it was

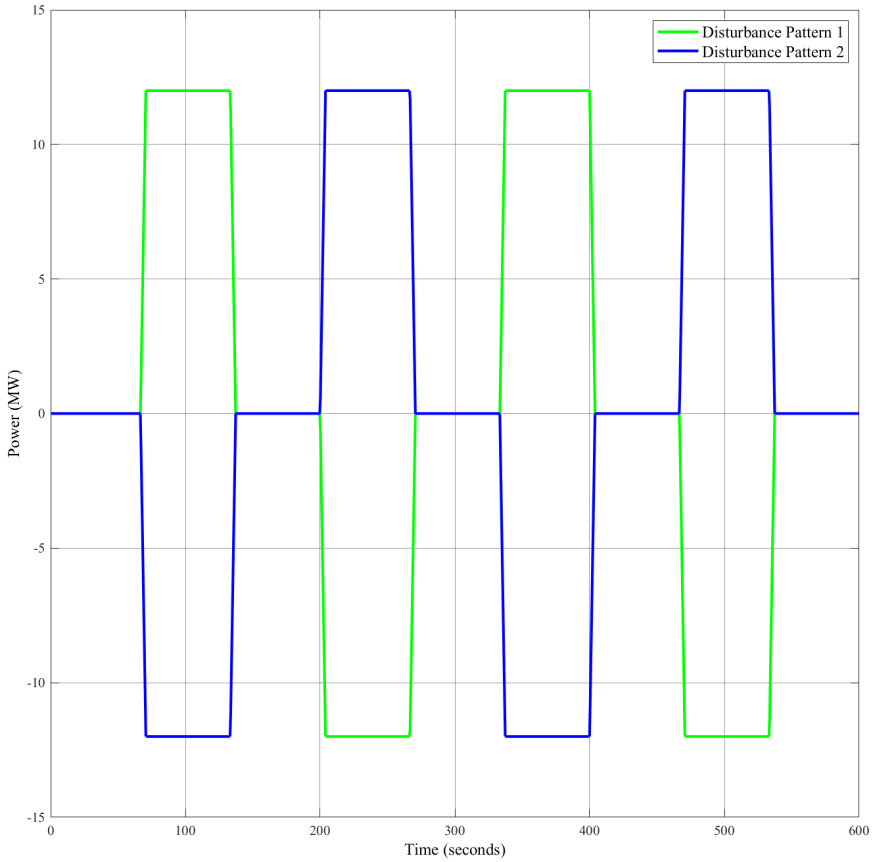

Figure 6.1 Load disturbance patterns.

arbitrarily chosen to have four disturbances throughout the simulation to keep the simulation simple. However, in order to keep the total load energy the same as in the undisturbed trials, it was necessary to apply an equal number of positive and negative load disturbances. To account for the variance in load levels in the different profiles, two disturbance patterns were generated, mirrored over the x-axis. Fourth, for duration of the disturbances, it was chosen to space the transition points equidistantly to reduce random effects from the different load profiles. The two load disturbance patterns are showing in Figure 6.1.

The complete results are shown in Figure 6.2. The disturbances break the implemented control on the energy storage that limits the overcharging, so these disturbances would cause issues in a physical system with over-injecting current to the

system. However, to keep a consistent measurement metric, the unserviced load is the considered factor in this testing.

Almost universally, the disturbances worsened the percentage of load that is not serviceable in each case. Due to the relatively consistent spread of peaks in the load throughout all the cases, this result is expected as it will increase the load above the threshold that the energy storage can handle.

Of particular interest are the cases in which the unserviced load decreases when one disturbance pattern is applied, while it increases with the other pattern. For instance, in Case 7 in the HP-ESOS, the first pattern results in 7.86 %, the second pattern results in 13.92 %, and the base load profile results in 10.85 % unserviced load. This pattern of decrease and increase is consistent in the PP-ESOS. In these instances, the base load is distributed in such a way that the different patterns can affect the same peak to a noticeable effect on the system, validating the choice to include the mirrored patterns. However, it is these cases that could cause the worst free circulating power, as the drop in load may exceed the capabilities of the generators to ramp down and thus overcharge the energy storage.

This evaluation shows the need for future developments in the model to mitigate the effects of disturbances. At best, unexpected load demand increases can simply cause an increase in unserviced load that can be resolved by disconnecting low-priority loads. However, a sudden drop in demand can cause dangerous free cycling currents in the power system. Effective disturbance mitigation techniques will be vital to reducing the chance of damaging the system.

6.2 Pulse Load Decision Matrix

While the pulse loads defined in Subsection 3.1.1 are randomly generated, they follow the same rules of construction. In a real system, it is possible for the pulse loads to have more varied magnitudes and durations. These differences would result in a

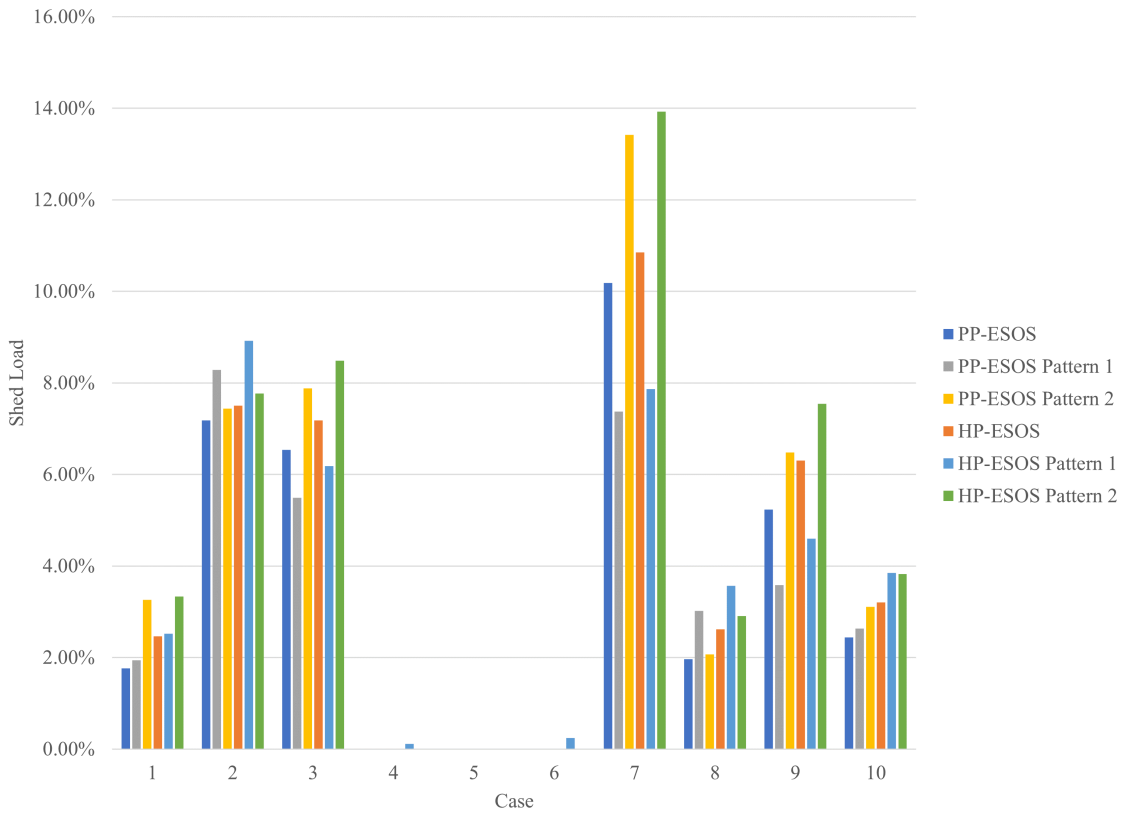

Figure 6.2 Comparison of ESOS results and results with disturbances.

change in the effect of the pulse load and also affect the profiles of the generators and energy storage devices. Thus, it is valuable to evaluate the trade-off between the energy of each pulse and the number of repeated pulses that the system is capable of producing.

For this evaluation, four pulse profiles were defined, summarized in Table 6.1. The full pulse uses the parameters established in Subsection 3.1.1. The second profile is one that is 75 % of the magnitude of a full pulse. As such, the magnitude of this pulse is 15 MW. Using the previously defined ramp rate, the rise and fall time of each pulse is reduced to 0.75 s. The duration of the peak magnitude and the duration between pulses are each held constant at 1 s. The third profile uses a magnitude of 50 % of a full pulse, with a magnitude of 10 MW and rise and fall times of 0.5 s. The final pulse

profile is 25 % of a full pulse, with a magnitude of 5 MW and rising and falling times of 0.25 s.

Table 6.1 Pulse Profile Definitions

Scale	Magnitude (MW)	Rise Time (s)	Peak Time (s)	Fall Time (s)	Wait Time (s)
100 %	20	1	1	1	1
75 %	15	0.75	1	0.75	1
50 %	10	0.5	1	0.5	1
25 %	5	0.25	1	0.25	1

These various profiles were tested in the model described in Section 3.3 with different settings for the constant base power of the system and initial state of charge. Each pulse profile was tested with the system at a baseline of 20 MW, 40 MW, 60 MW, 65 MW, 70 MW, 75 MW, and 80 MW. These tests were repeated with initial states of charge of 100 %, 80 %, 60 %, 40 %, and 20 %.

For the base powers less than 75 MW, the system was able to adjust the output of the generators high enough to offset the energy storage discharge from the pulses. This results in a theoretically infinite number of pulses that the system can produce. However, it also requires in an infeasible level of power injected into the system, either in the form of eventual overcharging the energy storage or introducing excess power into the bus. For the purpose of this evaluation, this infeasibility is negligible because future modifications to the system can eliminate this phenomenon. Additionally, this matrix is intended for decisions on a short and finite time scale when multiple pulse configurations might serve the same purpose. For instance, if a goal requires a pulse load to deliver 100 MJ of energy, this could be accomplished by 3 full pulses, 4 three-quarter pulses, 7 half pulses, or 16 quarter pulses, with all partial results rounded up.

The rest of the results are displayed in Table 6.2. At a base power of 75 MW, the half and quarter pulses can be produced infinitely due to the small magnitude

Table 6.2 Pulse Load Decision Matrix

Base Power (MW)	SoC (%)	100 % Pulse	75 % Pulse	50 % Pulse	25 % Pulse
75	100	20	137	∞	∞
75	80	16	109	∞	∞
75	60	11	82	∞	∞
75	40	7	54	∞	∞
75	20	3	27	∞	∞
80	100	7	12	26	94
80	80	5	9	21	75
80	60	4	7	15	56
80	40	2	4	10	37
80	20	1	2	5	18

exceeding the combined generator maximum of 82 MW. At a base power of 80 MW, all pulse profiles result in an eventual depletion of the energy storage. As can be noted, while the scaling of the pulse magnitude is linear, the feasible number of pulses at each magnitude is non-linear. This is due to the non-linear scaling of the energy content of each pulse due to the reduced rising and falling times.

While this decision matrix is not a definitive source due to the assumptions in construction, the numbers presented within can provide an approximation of the trade-off between the energy produced in a pulse and the number of pulses that can be produced by the system. This can be useful in any system that utilizes pulsed loads. In fabrication, arc furnaces create a pulsed load profile as they are used. By utilizing a decision matrix similar to this, facility operators could use integrated energy storage and decide on a fractional utilization of the facility that allows the energy storage to provide continuous benefit rather than needing to start and stop as the energy storage is charged and discharged.

Bibliography

[1] "Electricity generation, capacity, and sales in the united states - U.S. energy information administration (EIA)," https://www.eia.gov/energyexplained/electricity/electricity-in-the-us-generation-capacity-and-sales.php, accessed: 2021-8-22.

[2] W. Englund, "The grid's big looming problem: Getting power to where it's needed," *The Washington Post*, Jun. 2021.

[3] J. Dillon, "Transmission grid bottlenecks in northeast kingdom stall solar development," https://www.vpr.org/vpr-news/2020-12-15/transmission-grid-bottlenecks-in-northeast-kingdom-stall-solar-developmentstream/0, Dec. 2020, accessed: 2021-8-22.

[4] "Smart grid week: Working to modernize the nation's electric grid," https://www.energy.gov/articles/smart-grid-week-working-modernize-nation-s-electric-grid, accessed: 2021-8-22.

[5] "Grid-scale u.s. storage capacity could grow five-fold by 2050," https://www.nrel.gov/news/program/2021/grid-scale-storage-us-storage-capacity-could-grow-five-fold-by-2050.html, accessed: 2021-8-22.

[6] R. J. Campbell, "Weather-Related power outages and electric system resiliency," Aug. 2012.

[7] "Smart grid could reduce emissions by 12 percent," https://www.pnnl.gov/news/release.aspx?id=776, accessed: 2021-8-22.

[8] Z. Jin, G. Sulligoi, R. Cuzner, L. Meng, J. C. Vasquez, and J. M. Guerrero, "Next-Generation shipboard DC power system: Introduction smart grid and dc microgrid technologies into maritime electrical netowrks," *IEEE Electrification Magazine*, vol. 4, no. 2, pp. 45–57, Jun. 2016.

[9] N. R. Council, *NASA Space Technology Roadmaps and Priorities: Restoring NASA's Technological Edge and Paving the Way for a New Era in Space*. Washington, DC: The National Academies Press, 2012.

[10] M. Schluse, M. Priggemeyer, L. Atorf, and J. Rossmann, "Experimentable digital Twins—Streamlining Simulation-Based systems engineering for industry 4.0," *IEEE Trans. Ind. Inf.*, vol. 14, no. 4, pp. 1722–1731, Apr. 2018.

[11] "Digital twins for IoT applications: A comprehensive approach to implementing IoT digital twins," Oracle, Tech. Rep., Jan. 2017.

[12] A. Rasheed, O. San, and T. Kvamsdal, "Digital twin: Values, challenges and enablers from a modeling perspective," *IEEE Access*, vol. 8, pp. 21 980–22 012, 2020.

[13] E. Escorsa, "Digital twins: A glimpse at the main patented developments."

[14] W. Bellamy, III, "Boeing CEO talks 'digital twin' era of aviation," https://www.aviationtoday.com/2018/09/14/boeing-ceo-talks-digital-twin-era-aviation/, Sep. 2018, accessed: 2021-8-15.

[15] J. Coors-Blankenship, "How digital twins are raising the stakes on product development," https://www.industryweek.com/technology-and-iiot/article/21130033/how-digital-twins-are-raising-the-stakes-on-product-development, Apr. 2020, accessed: 2021-8-15.

[16] E. J. Tuegel, A. R. Ingraffea, T. G. Eason, and others, "Reengineering aircraft structural life prediction using a digital twin," *Aerosp. Eng.*, 2011.

[17] W. Danilczyk, Y. Sun, and H. He, "ANGEL: An intelligent digital twin framework for microgrid security," in *2019 North American Power Symposium (NAPS)*, Oct. 2019, pp. 1–6.

[18] F. Tao, H. Zhang, A. Liu, and A. Y. C. Nee, "Digital twin in industry: State-of-the-Art," *IEEE Trans. Ind. Inf.*, vol. 15, no. 4, pp. 2405–2415, Apr. 2019.

[19] D. Pomerantz, "The french connection: Digital twins from paris will protect wind turbines against battering north atlantic gales," https://www.ge.com/news/reports/french-connection-digital-twins-paris-will-protect-wind-turbines-battering-north-atlantic-gales, accessed: NA-NA-NA.

[20] D. Drazen, M. Vandroff, and L. Tarasek, "Cyber-Physical systems: Navy digital twin," Nov. 2018.

[21] S. Kanowitz, "How digital twins keep navy ahead on ship maintenance," https://gcn.com/articles/2020/05/01/navy-digital-twin-ship-maintenance.aspx, May 2020, accessed: NA-NA-NA.

[22] "Electrical digital twin," https://new.siemens.com/global/en/products/energy/energy-automation-and-smart-grid/electrical-digital-twin.html, Apr. 2021, accessed: 2021-8-15.

[23] M. Engelhardt, "How do you know where to invest in your power grid?" https://new.siemens.com/global/en/company/stories/infrastructure/2018/digital-twin-fingrid.html, Jun. 2021, accessed: 2021-8-15.

[24] M. Zhou and J. Yan, "A new solution architecture for online power system analysis," *CSEE Journal of Power and Energy Systems*, vol. 4, no. 2, pp. 250–256, Jun. 2018.

[25] M. Zhou and D. Feng, "Application of In-Memory computing to online power grid analysis," *IFAC-PapersOnLine*, vol. 51, no. 28, pp. 132–137, Jan. 2018.

[26] M. Zhou, J. Yan, and D. Feng, "Digital twin framework and its application to power grid online analysis," *CSEE Journal of Power and Energy Systems*, vol. 5, no. 3, pp. 391–398, Sep. 2019.

[27] M. Zhou and D. Feng, "Parallel contingency analysis for Multi-CPU/Core computing environment," in *IFAC Workshop on Control of Smart Grid and Renewable Energy Systems (CSGRES 2019)*. unknown, May 2019.

[28] R. H. Lasseter, "Microgrids," in *2002 IEEE Power Engineering Society Winter Meeting. Conference Proceedings (Cat. No. 02CH37309)*, vol. 1. IEEE, 2002, pp. 305–308.

[29] J. A. P. Lopes, A. G. Madureira, and C. C. L. M. Moreira, "A view of microgrids," *Wiley Interdiscip. Rev. Energy Environ.*, vol. 2, no. 1, pp. 86–103, Jan. 2013.

[30] J. M. Guerrero, J. C. Vasquez, J. Matas, L. G. de Vicuna, and M. Castilla, "Hierarchical control of Droop-Controlled AC and DC Microgrids—A general approach toward standardization," *IEEE Trans. Ind. Electron.*, vol. 58, no. 1, pp. 158–172, Jan. 2011.

[31] D. Kumar, F. Zare, and A. Ghosh, "DC microgrid technology: System architectures, AC grid interfaces, grounding schemes, power quality, communication

networks, applications, and standardizations aspects," *IEEE Access*, vol. 5, pp. 12 230–12 256, 2017.

[32] A. Pratt, P. Kumar, and T. V. Aldridge, "Evaluation of 400V DC distribution in telco and data centers to improve energy efficiency," in *INTELEC 07 - 29th International Telecommunications Energy Conference*, Sep. 2007, pp. 32–39.

[33] T. Dragičević, X. Lu, J. C. Vasquez, and J. M. Guerrero, "DC Microgrids—Part II: A review of power architectures, applications, and standardization issues," *IEEE Trans. Power Electron.*, vol. 31, no. 5, pp. 3528–3549, May 2016.

[34] A. T. Elsayed, A. A. Mohamed, and O. A. Mohammed, "DC microgrids and distribution systems: An overview," *Electric Power Systems Research*, vol. 119, pp. 407–417, Feb. 2015.

[35] V. Vossos, K. Garbesi, and H. Shen, "Energy savings from direct-DC in U.S. residential buildings," *Energy Build.*, vol. 68, pp. 223–231, Jan. 2014.

[36] J. A. P. Lopes, C. L. Moreira, and A. G. Madureira, "Defining control strategies for MicroGrids islanded operation," *IEEE Trans. Power Syst.*, vol. 21, no. 2, pp. 916–924, May 2006.

[37] N. Doerry, J. Amy, and C. Krolick, "History and the status of electric ship propulsion, integrated power systems, and future trends in the U.S. navy," *Proc. IEEE*, vol. 103, no. 12, pp. 2243–2251, Dec. 2015.

[38] N. Doerry and H. Fireman, "Designing all electric ships," 01 2006.

[39] C. N. H. Doerry, "Next generation integrated power systems for the future fleet," http://www.doerry.org/norbert/papers/090106usna-ngips-final.pdf, accessed: 2021-2-19.

[40] J. Kuseian, "Naval power systems technology roadmap," Electric Ships Office, Tech. Rep., 2013.

[41] G. Chang, Y. Wu, S. Shao, Z. Huang, and T. Long, "DC bus systems for electrical ships," *IEEE Electrification Magazine*, vol. 8, no. 3, pp. 28–39, Sep. 2020.

[42] D. Deng, "Li-ion batteries: basics, progress, and challenges," *Energy Sci. Eng.*, vol. 3, no. 5, pp. 385–418, Sep. 2015.

[43] K. Smith, "Design of electric drive vehicle batteries for long life and low cost: Robustness to geographic and Consumer-Usage variation," IEEE 2010 Workshop on Accelerated Stress Testing and Reliability, 2010.

[44] G. Ning and B. N. Popov, "Cycle life modeling of Lithium-Ion batteries," *J. Electrochem. Soc.*, vol. 151, no. 10, p. A1584, Sep. 2004.

[45] T. Guena and P. Leblanc, "How depth of discharge affects the cycle life of Lithium-Metal-Polymer batteries," in *INTELEC 06 - Twenty-Eighth International Telecommunications Energy Conference*, Sep. 2006, pp. 1–8.

[46] H. de Vries, T. T. Nguyen, and B. Op het Veld, "Increasing the cycle life of lithium ion cells by partial state of charge cycling," *Microelectron. Reliab.*, vol. 55, no. 11, pp. 2247–2253, Nov. 2015.

[47] S. S. Choi and H. S. Lim, "Factors that affect cycle-life and possible degradation mechanisms of a li-ion cell based on LiCoO2," *J. Power Sources*, vol. 111, no. 1, pp. 130–136, Sep. 2002.

[48] I. Bloom, B. W. Cole, J. J. Sohn, S. A. Jones, E. G. Polzin, V. S. Battaglia, G. L. Henriksen, C. Motloch, R. Richardson, T. Unkelhaeuser, D. Ingersoll, and H. L. Case, "An accelerated calendar and cycle life study of li-ion cells," *J. Power Sources*, vol. 101, no. 2, pp. 238–247, Oct. 2001.

[49] D. K. Molzahn, "Identifying and characterizing Non-Convexities in feasible spaces of optimal power flow problems," *IEEE Trans. Circuits Syst. Express Briefs*, vol. 65, no. 5, pp. 672–676, May 2018.

[50] J. A. Momoh, R. Adapa, and M. E. El-Hawary, "A review of selected optimal power flow literature to 1993. i. nonlinear and quadratic programming approaches," *IEEE Trans. Power Syst.*, vol. 14, no. 1, pp. 96–104, 1999.

[51] J. A. Momoh, M. E. El-Hawary, and R. Adapa, "A review of selected optimal power flow literature to 1993. II. newton, linear programming and interior point methods," *IEEE Trans. Power Syst.*, vol. 14, no. 1, pp. 105–111, Feb. 1999.

[52] J. Lavaei and S. H. Low, "Zero duality gap in optimal power flow problem," *IEEE Trans. Power Syst.*, vol. 27, no. 1, pp. 92–107, Feb. 2012.

[53] P. Kankanala, S. C. Srivastava, A. K. Srivastava, and N. N. Schulz, "Optimal control of voltage and power in a Multi-Zonal MVDC shipboard power system," *IEEE Trans. Power Syst.*, vol. 27, no. 2, pp. 642–650, May 2012.

[54] X. Pan, T. Zhao, and M. Chen, "DeepOPF: Deep neural network for DC optimal power flow," May 2019.

[55] J. Duncan Glover, T. Overbye, and M. S. Sarma, *Power System Analysis and Design.* Cengage Learning, Jan. 2016.

[56] J. S. Arora, *Introduction to Optimum Design*, ser. Third Edition. Elsevier Inc., 2012.

[57] T. W. Price, "A multiagent energy management control system for commercial and industrial applications," Ph.D. dissertation, University of South Carolina, 2012.

[58] H. Park, J. Sun, S. Pekarek, P. Stone, D. Opila, R. Meyer, I. Kolmanovsky, and R. DeCarlo, "Real-Time model predictive control for shipboard power management using the IPA-SQP approach," *IEEE Trans. Control Syst. Technol.*, vol. 23, no. 6, pp. 2129–2143, Nov. 2015.

[59] M. Leonard-Albert, D. Hobbs, J. Hannum, E. Santi, and K. Booth, "Early stage modeling of naval DC power system for digital twin development," in *2021 IEEE Electric Ship Technologies Symposium (ESTS)*, Aug. 2021, pp. 1–8.

[60] G. L. Sinsley, D. F. Opila, E. S. Oh, and J. D. Stevens, "Upper bound performance of shipboard power and energy systems for Early-Stage design," *IEEE Access*, vol. 8, pp. 178 600–178 613, 2020.

[61] M. Sechilariu, B. C. Wang, F. Locment, and A. Jouglet, "DC microgrid power flow optimization by multi-layer supervision control. design and experimental validation," *Energy Convers. Manage.*, vol. 82, pp. 1–10, Jun. 2014.

[62] Chief of Naval Operations, *OPNAV Instruction 3501.352A*, US Department of the Navy, Apr. 2014.

[63] P. Keil and A. Jossen, "Charging protocols for lithium-ion batteries and their impact on cycle life—an experimental study with different 18650 high-power cells," *Journal of Energy Storage*, vol. 6, pp. 125–141, May 2016.

[64] Y. Cengel, *Heat and Mass Transfer: Fundamentals and Applications.* McGraw-Hill Higher Education, 2014.